Letter

Highly Doped Upconversion Nanoparticles for In Vivo Applications Under Mild Excitation Power

Du Li, Shihui Wen, Mengya Kong, Yongtao Liu, Wei Hu, Bingyang Shi, Xiangyang Shi, and Dayong Jin

Anal. Chem., **Just Accepted Manuscript** • DOI: 10.1021/acs.analchem.0c02143 • Publication Date (Web): 29 Jul 2020

Highly Doped Upconversion Nanoparticles for *In Vivo* Applications Under Mild Excitation Power

Du Li[1,2], Shihui Wen[1*], Mengya Kong[3], Yongtao Liu[1], Wei Hu[2], Bingyang Shi[4], Xiangyang Shi[2*] and Dayong Jin[1,5*]

[1]Institute for Biomedical Materials and Devices (IBMD), Faculty of Science, University of Technology Sydney, NSW 2007, Australia

[2]College of Chemistry, Chemical Engineering and Biotechnology, Donghua University, Shanghai 201620, People's Republic of China

[3]Department of Chemistry & Institutes of Biomedical Sciences & State Key Laboratory of Molecular Engineering of Polymers, Fudan University, Shanghai, China.

[4]Department of Biomedical Sciences, Faculty of Medicine & Health Sciences, Macquarie University, Sydney, New South Wales 2109, Australia

[5]UTS-SUStech Joint Research Centre for Biomedical Materials & Devices, Department of Biomedical Engineering, Southern University of Science and Technology, Shenzhen, China

E-mail: shihui.wen@uts.edu.au (**S. Wen**), xshi@dhu.edu.cn (**X. Shi**) and dayong.jin@uts.edu.au (**D. Jin**)

One of the major challenges in using upconversion nanoparticles (UCNPs) is to improve their brightness. This is particularly true for *in vivo* studies, as the low power excitation is required to prevent the potential photo toxicity to live cells and tissues. Here, we report that the typical $NaYF_4$:$Yb_{0.2}$,$Er_{0.02}$ nanoparticles can be highly doped, and the formula of $NaYF_4$:$Yb_{0.8}$,$Er_{0.06}$ can gain orders of magnitude more brightness, which is applicable to a range of mild 980 nm excitation power densities, from 0.005 W/cm² to 0.5 W/cm². Our results reveal that the concentration of Yb^{3+} sensitizer ions plays an essential role, while increasing the doping concentration of Er^{3+} activator ions to 6 mol% only has incremental effect. We further demonstrated a type of bright UCNPs 12 nm in total diameter for *in vivo* tumor imaging at a power density as low as 0.0027 W/cm², bringing down the excitation power requirement by 42 times. This work re-defines the doping concentrations to fight for the issue of concentration quenching, so that ultra-small and bright nanoparticles can be used to further improve the performance of upconversion nanotechnology in photodynamic therapy, light-triggered drug release, optogenetics, and night vision enhancement.

Upconversion materials can absorb two or more near-infrared (NIR) photons and emit shorter wavelength luminescence in the visible and ultraviolet (UV) [1-3]. Such a fascinating anti-Stokes property has led to a broad range of optoelectronics applications, including full-colour displays [4], security inks[5], photocatalysis [6], and photovoltaics [7]. By taking the advantage of NIR deep penetration through the tissue as well as their exceptional photo stability, long decaying lifetimes[8], large anti-stoke shifts and sharp emission spectra, the emerging field of lanthanide doped upconversion nanoparticles (UCNPs) has attracted a great deal of interests in bio-imaging[9-12], light-controlled nanomedicine[3, 13-16] and NIR night vision enhancement [17].

One of the major challenges to transform upconversion nanotechnology is to reduce the excitation power requirement and improve the brightness of UCNPs. Due to the constraint of concentration quenching, the dopant concentrations are restricted at relatively low levels, e.g. 20 mol% Yb^{3+} as sensitizers and 2 mol% Er^{3+} or 0.5 mol% Tm^{3+} as activators [18, 19], to minimize luminescence quenching effects. In 2013, we reported that highly Tm^{3+}-doped UCNPs can display exceptionally high brightness,

where high excitation power (up to ~ 10^6 W/cm^2) was necessary to mitigate concentration quenching [20]. Significant efforts have been made to improve the brightness of UCNPs by increasing the doping concentrations of sensitizers and activators[21-23]. Remarkably, Steven Chu's group recently reported that highly Yb^{3+} and Er^{3+} doped nanocrystals exhibit a 150-fold enhancement at 8 W/cm^2 using an inert shell strategy[22], and in parallel, the team led by Cohen, Chan, and Schuck at Berkeley reported that alloyed UCNPs can realize a deep-tissue imaging under the excitation power of 0.1 W/cm^2 [21].

Low-power excitation is required for the safe *in vivo* applications, e.g. the power densities in the range of 0.001 to 0.5 W/cm^2 are needed for bioimaging[10], NIR-triggered drug release[3], photodynamic therapy[14, 24], and night vision enhancement[17]. This gap between the high brightness and low power excitation becomes more evident when the size of UCNPs is within 15 nm, where the number of dopants per nanoparticles proportionally drops and surface quenching inevitably arises [25, 26].

Here, we find that the concentrations of both Yb^{3+} sensitizers and Er^{3+}activators can be further fine-tuned and gain the significant enhancement in the brightness of UCNPs for in vivo applications when only mild to ultra-low irradiance are required. We adopt here a series of controlled synthesis of core@shell@shell UCNPs ($NaYF_4$@$NaYF_4$:Yb_x,Er_y@$NaYF_4$) to exclude the size effect, so that the influences of sensitizers' and activators' concentrations on the brightness of multi-colour upconversion emission can be systematically compared and quantified at a range of laser irradiance. For example, under an irradiance of 0.082 W/cm^2, compared with the widely-used $NaYF_4$:$Yb_{0.2}$,$Er_{0.02}$ ones, the new formula of $NaYF_4$:$Yb_{0.8}$,$Er_{0.06}$, yields the luminescence enhancements of 75.3, 40.8, 10.0, and 37.0 folds in ultraviolet, violet, green, and red emissions, respectively. This has further guided us to achieve a new type of 12 nm highly-doped core-shell UCNPs with much enhanced red emissions for in vivo imaging using an excitation irradiance as low as 0.0027 W/cm^2.

To quantify the roles of the concentrations of sensitizer ions and activator ions in enhancing the brightness of UCNPs, it requires the size of single UCNPs should be identical. Due to the difference in crystalline unit cells, the changes of Yb^{3+} concentrations, particularly at high levels, can significantly affect the overall size of nanoparticles when they are synthesized by the conventional coprecipitation method [23]. Therefore, we use an inert $NaYF_4$ core as the template and design a heterogeneous sandwich structure of inert-core@active-shell@inert-shell nanoparticles (**Fig. 1a-c**), so that the Yb^{3+} and Er^{3+}

concentrations can be arbitrarily tuned within the same volume of the active shell in the middle. The role of the inert $NaYF_4$ shell is to minimize non-radiative energy loss by preventing the exciton energy transfer to the surface defects and surrounding solvents via Yb^{3+} ions.

As shown in **Fig. 1b-c**, transmission electronic microscopy (TEM) images show the typical batches of highly uniform nanocrystals of $NaYF_4$, $NaYF_4$@$NaYF_4$:$Yb_{0.2}$,$Er_{0.02}$, and $NaYF_4$@$NaYF_4$:$Yb_{0.2}$,$Er_{0.02}$@$NaYF_4$, synthesized by the layer-by-layer hot injection method [27]. The sizes of core, core@shell, and core@shell@shell nanoparticles are 18 nm, 28 nm and 34 nm, respectively, indicating 5 nm active shell and 3 nm inert shell (**Fig. S1**). With the increase doping concentration of bother Yb^{3+} (80%) and Er^{3+} (6%) in the active shell, we get the highly doped core@shell@shell nanoparticles with the similar size (**Fig. 1b-c**). The actual concentrations of Y^{3+}, Yb^{3+} and Er^{3+} of core@shell@shell nanoparticles are further characterized by using inductively coupled plasma mass spectrometry. The molar ratios of Y/Yb/Er in active shell of $NaYF_4$@$NaYF_4$:$Yb_{0.2}$,$Er_{0.02}$@$NaYF_4$ and $NaYF_4$@$NaYF_4$:$Yb_{0.8}$,$Er_{0.06}$@$NaYF_4$ have been calculated to be 0.79:0.19:0.018 and 0.15:0.78:0.063, respectively, which confirms that rare earth compositions of UCNP consistent to their feeding ratio. Also, all the synthesized nanoparticles are uniform with narrow size distributions (**Fig. S1**), which supports the following quantitative comparisons of the upconversion luminescence intensities. As shown in **Fig. 1d**, the luminescence spectra of as-synthesized UCNPs have four characteristic peaks at 379 nm (ultraviolet), 407 nm (violet), 540 nm (green) and 650 nm (red), assigned to $^4G_{11/2} \rightarrow {}^4I_{15/2}$, $^2H_{9/2} \rightarrow {}^4I_{15/2}$, $^2H_{11/2}/{}^4S_{3/2} \rightarrow {}^4I_{15/2}$ and $^4F_{9/2} \rightarrow {}^4I_{15/2}$ transitions of Er^{3+}, respectively. Quantitatively, highly doped $NaYF_4$@$NaYF_4$:$Yb_{0.8}$,$Er_{0.06}$@$NaYF_4$ nanoparticles result in 39, 24, 6.4, and 21 fold brightness enhancements in ultraviolet, violet, green, and red, compared with the $NaYF_4$@$NaYF_4$:$Yb_{0.2}$,$Er_{0.02}$@$NaYF_4$ nanocrystals under the excitation power of 0.25 W/cm^2.

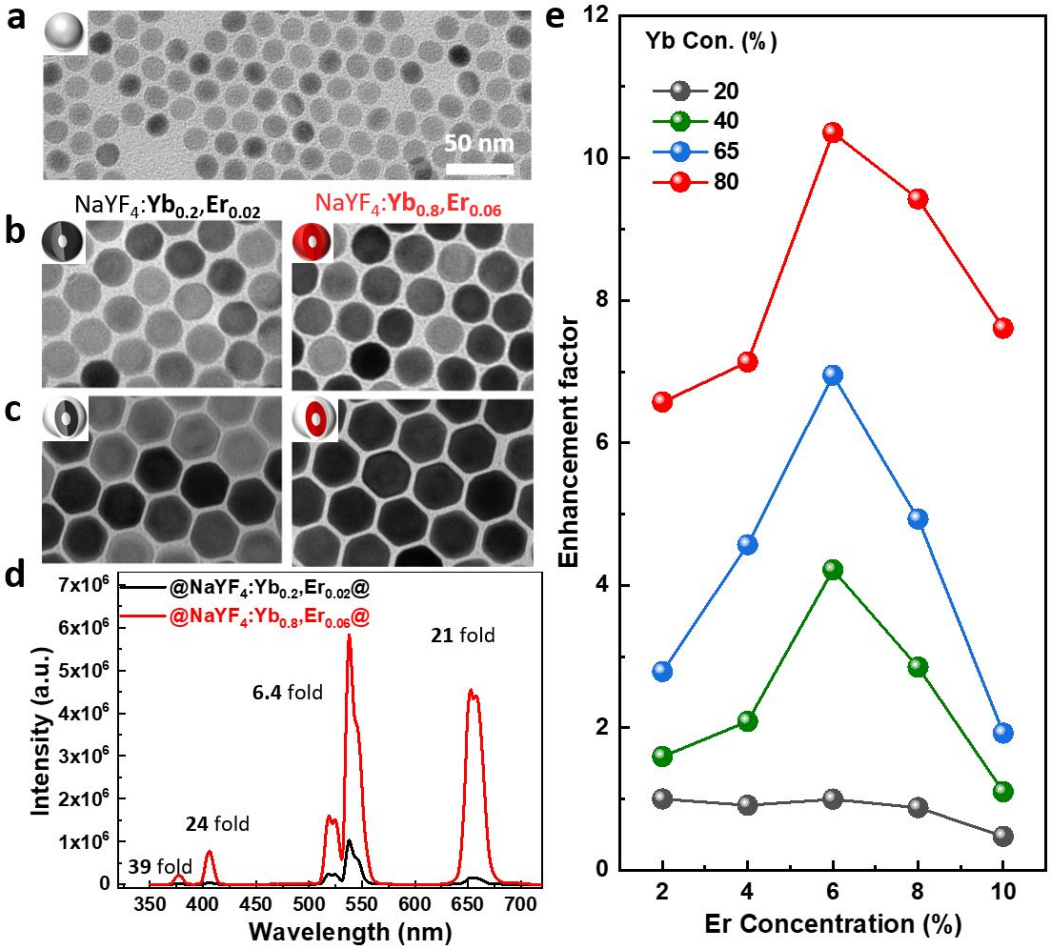

Figure 1. TEM images of $NaYF_4$ core (**a**), $NaYF_4$@$NaYF_4$:$Yb_{0.2}$,$Er_{0.02}$ (**b**, left), $NaYF_4$@$NaYF_4$:$Yb_{0.8}$,$Er_{0.06}$ (**b**, right), $NaYF_4$@$NaYF_4$:$Yb_{0.2}$,$Er_{0.02}$@$NaYF_4$ (**c**, left), and $NaYF_4$@$NaYF_4$:$Yb_{0.8}$,$Er_{0.06}$@$NaYF_4$ (**c**, right), the scale bar is 50 nm. (**d**) Luminescence spectra of $NaYF_4$@$NaYF_4$:$Yb_{0.8}$,$Er_{0.06}$@$NaYF_4$ and $NaYF_4$@$NaYF_4$:$Yb_{0.2}$,$Er_{0.02}$@$NaYF_4$ under the excitation power of 0.25 W/cm^2, (**e**) Integrated luminescence intensity enhancement of $NaYF_4$@$NaYF_4$:Yb_x,Er_y@$NaYF_4$ samples compared with $NaYF_4$@$NaYF_4$:$Yb_{0.2}$,$Er_{0.02}$@$NaYF_4$ under the excitation power of 0.25 W/cm^2.

We then systematically synthesize a series of 20 batches of UCNPs doped with different dopant combinations of sensitizer (x) and activator (y) and study their optical properties. We orthogonally apply four different Yb^{3+} concentrations (x = 20%, 40%, 65% and 80%) and five different Er^{3+} dopant concentrations (y = 2%, 4%, 6%, 8% and 10%). All the nanoparticles have the same structure and size as confirmed by the TEM results (**Fig. S2-5**). As shown in **Fig. 1e**, the brightness of UCNPs increases with an increase of Yb^{3+} from 20% to 80% when fixing the doping concentration of Er^{3+}, which is due to both the elevated photon harvest efficiency of the sensitizers and the reduced distance between donor and acceptor, as energy transfer rate is proportional to d^{-6} in dipole–dipole interaction (d refers to the average donor–acceptor distance) [28]. The luminescence intensity first enhances with ascended

Er^{3+} concentration from 2% to 6% and then declines with the Er^{3+} concentration above 6%, showing a sign of the cross-relaxation induced energy loss. By fixing the Er^{3+} concentration at 6%, we further increase the Yb^{3+} concentration to 94% (**Fig. S6**), and find that the luminescence intensity of $NaYF_4$@$NaYbF_4$:$Er_{0.06}$@$NaYF_4$ is lower than that of $NaYF_4$@$NaYF_4$:$Yb_{0.8}$,$Er_{0.06}$@$NaYF_4$ (**Fig. S7**), which is consistent to the previous report.[29] To further study the effect of Yb^{3+} concentration on the energy transfer process, we examine the time-resolved green emission of the samples with different Yb^{3+} concentrations. As shown in **Fig. S8**, the luminescence lifetime decreases from 252 to 99 μs as the Yb^{3+} concentration increases from 20% to 94%, which indicates the back-energy-transfer process from Er^{3+} to Yb^{3+} in the highly doped samples. Therefore, the optimal Yb^{3+} concentration at 80% is to balance the effects of increasing absorption and reducing back-energy-transfer.

The luminescence enhancement of UCNPs can be strongly power-dependent. As shown in **Fig. 2a**, when the excitation power density increases from 0.25 W/cm^2 to 0.5 W/cm^2, the enhancement factors slightly decrease from 39, 24, 6.4, and 21 folds to 23, 13, 3.7, and 19 folds, at the ultraviolet, violet, green, and red emission bands, respectively. When the excitation power density decreases to 0.005 W/cm^2, the enhancement by the highly doped UCNPs is more obvious, e.g. 16 folds at the green band (**Fig. 2b**). To further understand the brightness enhancement of highly doped UCNPs, we systemically conduct power dependent luminescence measurements in the range of 0.005 to 0.5 W/cm^2, integrate the emissions from different bandwidth (**Fig. S9**) and further calculated the enhancement factors, as shown in **Fig. 2c**. The emission intensity ratio at 407 nm increases from 13.0 to 49.0 when the irradiance decreases from 0.5 to 0.062 W/cm^2. Similarly, luminescence enhancement at 379 nm increases around 3 times and achieves 75.3 at the irradiance of 0.081 W/cm^2. Also, the brightness enhancement factors of green and red luminescence (540 nm and 650 nm) increase from 3.7 and 19.0 to 15.2 and 38.0, respectively, when the irradiance reduces from 0.5 to 0.016 W/cm^2. This trend is consistent with the increased probability of highly efficient energy absorption of the highly Yb^{3+}-doped UCNPs at relatively low irradiance.

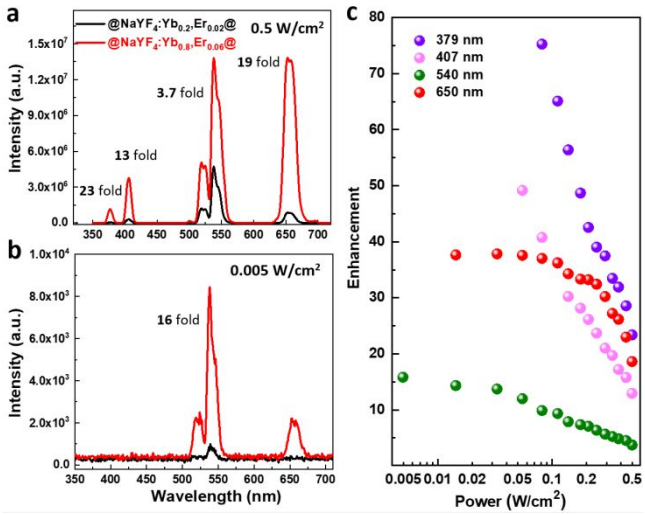

Figure 2. Luminescence spectra of $NaYF_4$@$NaYF_4$:$Yb_{0.8}$,$Er_{0.06}$@$NaYF_4$ and $NaYF_4$@$NaYF_4$:$Yb_{0.2}$,$Er_{0.02}$@$NaYF_4$ under the irradiance of 0.5 W/cm² (**a**) and 0.005 W/cm² (**b**). (**c**) Comparison of power-dependent luminescence intensity enhancements between $NaYF_4$@$NaYF_4$:$Yb_{0.8}$,$Er_{0.06}$@$NaYF_4$ and $NaYF_4$@$NaYF_4$:$Yb_{0.2}$,$Er_{0.02}$@$NaYF_4$ at UV (379 nm), violet (407 nm), green (540 nm), and red (650 nm) bands, respectively.

We determine that the sensitizers' concentration dominates the power-dependent properties, as shown in **Fig. 3**. For the highly Yb^{3+}-doped $NaYF_4$@$NaYF_4$:$Yb_{0.8}$,$Er_{0.02}$@$NaYF_4$ nanoparticles, the brightness enhancement factors across all the emission bands significantly increase with the decrease of irradiance (**Fig. 3a**). For example, the enhancement factors of the UV emissions increase significantly from 17.1 to 52.5. In contrast, the irradiance has negligible effect in the brightness enhancement factors for the highly Er^{3+}-doped $NaYF_4$@$NaYF_4$:$Yb_{0.2}$,$Er_{0.06}$@$NaYF_4$ nanoparticles (**Fig. 3b**). Similarly, with the optimal Yb^{3+} concentration of 80%, the increase of Er^{3+} doping concentration from 2% to 6% only slightly increases the luminescence with the enhancement factor around 1.8 (**Fig. 3c**). Also, the enhancement factors do not change with the excitation power density. These results suggest the increased NIR photon sensitization becomes critical to increase the brightness of highly doped UCNPs under the mild and low irradiance conditions.

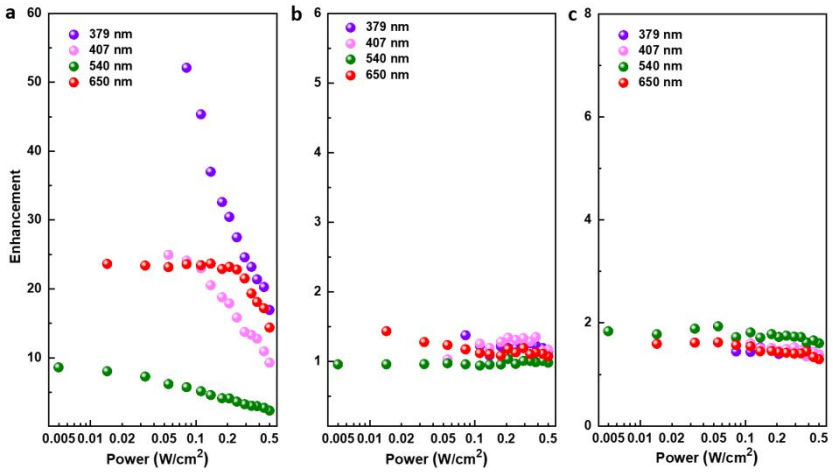

Figure 3. The power-dependent upconversion enhancement factors for $NaYF_4$@$NaYF_4$:$Yb_{0.8}$,$Er_{0.02}$@$NaYF_4$ compared with $NaYF_4$@$NaYF_4$:$Yb_{0.2}$,$Er_{0.02}$@$NaYF_4$ (**a**), $NaYF_4$@$NaYF_4$:$Yb_{0.2}$,$Er_{0.06}$@$NaYF_4$ compared with $NaYF_4$@$NaYF_4$:$Yb_{0.2}$,$Er_{0.02}$@$NaYF_4$ (**b**), and $NaYF_4$@$NaYF_4$:$Yb_{0.8}$,$Er_{0.06}$@$NaYF_4$ compared with $NaYF_4$@$NaYF_4$:$Yb_{0.8}$,$Er_{0.02}$@$NaYF_4$ (**c**) at different emission bands.

We then survey the broad range of demonstrated *in vivo* applications using the conventional $NaYF_4$:$Yb_{0.2}$,$Er_{0.02}$@$NaYF_4$ UCNPs, as summarized in **Table 1**. We anticipate that the new formula of highly doped UCNPs will immediately offer at least one order of magnitude brightness enhancement or to achieve the same performance with a much reduced irradiance. For bioimaging, the red upconversion emissions are the preferable due to the less extinction through the tissues [10, 30], therefore the enhancement factor of 37 in red band using the $NaYF_4$:$Yb_{0.8}$,$Er_{0.06}$@$NaYF_4$ will significantly improve the imaging sensitivity. Similarly, the improved photodynamic therapy treatment will be achieved by using the $NaYF_4$:$Yb_{0.8}$,$Er_{0.06}$@$NaYF_4$, as the red emission from Er^{3+}-doped UCNPs is commonly used to active photosensitizer (Zinc phthalocyanine)[14, 24]. For NIR light-triggered drug release, the green emission of $NaYF_4$:$Yb_{0.2}$,$Er_{0.02}$@$NaYF_4$ could be used to photolysis Roussin's black salt to generate NO under the excitation power of 5-30 W/cm^2 [3, 31]. Also, relatively high excitation power (0.5-400 W/cm^2) is needed for $NaYF_4$:$Yb_{0.2}$,$Er_{0.02}$@$NaYF_4$ to generate the strong green light for optogenetics applications[13, 32]. With the usage of $NaYF_4$:$Yb_{0.8}$,$Er_{0.06}$@$NaYF_4$, the excitation power could be significantly reduced for safety in vivo drug delivery and optogenetics applications. Recently, Ma et al. developed ocular injectable photoreceptor-binding UCNPs to extend the mammalian visual spectrum into the NIR range under the excitation power of 0.0016 W/cm^2 [17]. We anticipate the new doping formula will improve the green emission for around 15 times and significantly improve the

sensitivity to the NIR light.

Table 1. A summary of the anticipated improvements for the highly doped UCNPs in bio applications

Recommended applications	Upconversion nanoparticles	Desirable emission band	Irradiance range	Ref.	Anticipated improvement if using the new doping formula
In vivo bio-imaging	$NaYF_4:Yb_{0.2},Er_{0.02}$	Red (600 ~ 700 nm)	0.12 W/cm^2	30	38 times luminescence enhancement
Photodynamic therapy	$NaYF_4:Yb_{0.2},Er_{0.02}$	Red (~650 nm)	0.39-0.415 W/cm^2	14, 24	26 times luminescence enhancement or reduce the irradiance to < 0.1 W/cm^2
Drug release and delivery	$NaYF_4:Yb_{0.25},Er_{0.02}$	Green (510 ~ 560 nm)	0.5-400 W/cm^2	31	~ 15 times luminescence enhancement or reduce the irradiance to < 0.5 W/cm^2
Optogenetics	$NaYF_4:Yb_{0.2},Er_{0.02}$ @$NaYF_4$	Green (510 ~ 560 nm)	0.44-140 W/cm^2	13, 32	~ 10 times luminescence enhancement or reduce the irradiance to < 0.8 W/cm^2
Night vision enhancement	$NaYF_4:Yb_{0.2},Er_{0.02}$ @$NaYF_4$	Green (~550 nm)	0.0016 W/cm^2	17	~ 15 times luminescence enhancement

We further validate the advantage of the highly doped UCNPs for *in vivo* tumor imaging. In this experiment, as ideal nanoparticles with the smaller size are preferred due to higher efficiency in cargos delivery, and their improved body clearance and biocompatibility[33], we simplify our design into $NaYF_4:Yb_{0.8},Er_{0.06}@NaYF_4$ so that smaller sized highly doped UCNPs can be synthesized. The $NaYF_4:Yb_{0.8},Er_{0.06}$ active cores display a narrow size distribution with an average diameter of 8.6 nm, and the final size of $NaYF_4:Yb_{0.8},Er_{0.06}@NaYF_4$ is measured to be 11.9 nm (**Fig. S10a-b**), smaller than the size of dye-labelled IgG antibody[34]. It should be noted that the formula of $NaYF_4:Yb_{0.8},Er_{0.06}@NaYF_4$ UCNPs displays the enhanced emission compared with that with low doping concentrations (**Fig. S10c**), suggesting that the optimal concentrations of Yb^{3+} and Er^{3+} ions are independent on the size of the nanoparticles.

To demonstrate the improved brightness and tissue penetration ability of the 12 nm highly doped UCNPs, we first test them underneath the pork tissue (**Fig. S11**). As shown in **Fig. 4a-b**, using an irradiance of 0.5 W/cm^2, the strong 660 nm band upconversion image of $NaYF_4:Yb_{0.8},Er_{0.06}@NaYF_4$ can be detected at a tissue depth of 4.0 mm, while the signal of conventional

$NaYF_4$:$Yb_{0.2}$,$Er_{0.02}$@$NaYF_4$ UCNPs can only penetrate 1.0 mm. Quantitatively, the signal to noise ratio (SNR) of $NaYF_4$:$Yb_{0.8}$,$Er_{0.06}$@$NaYF_4$ covered by 1 mm pork tissue is around 20, which is 5 times higher than the SNR of $NaYF_4$:$Yb_{0.2}$,$Er_{0.02}$@$NaYF_4$ UCNPs (**Fig. 4c**). The penetration ability of green luminescent signals from both $NaYF_4$:$Yb_{0.8}$,$Er_{0.06}$@$NaYF_4$ and $NaYF_4$:$Yb_{0.2}$,$Er_{0.02}$@$NaYF_4$ is relative weak, as the green SNR of $NaYF_4$:$Yb_{0.8}$,$Er_{0.06}$@$NaYF_4$ covered by 1 mm pork tissue is 6.1 while the SNR of $NaYF_4$:$Yb_{0.2}$,$Er_{0.02}$@$NaYF_4$ UCNPs is only 1.5 (**Figure S12**).

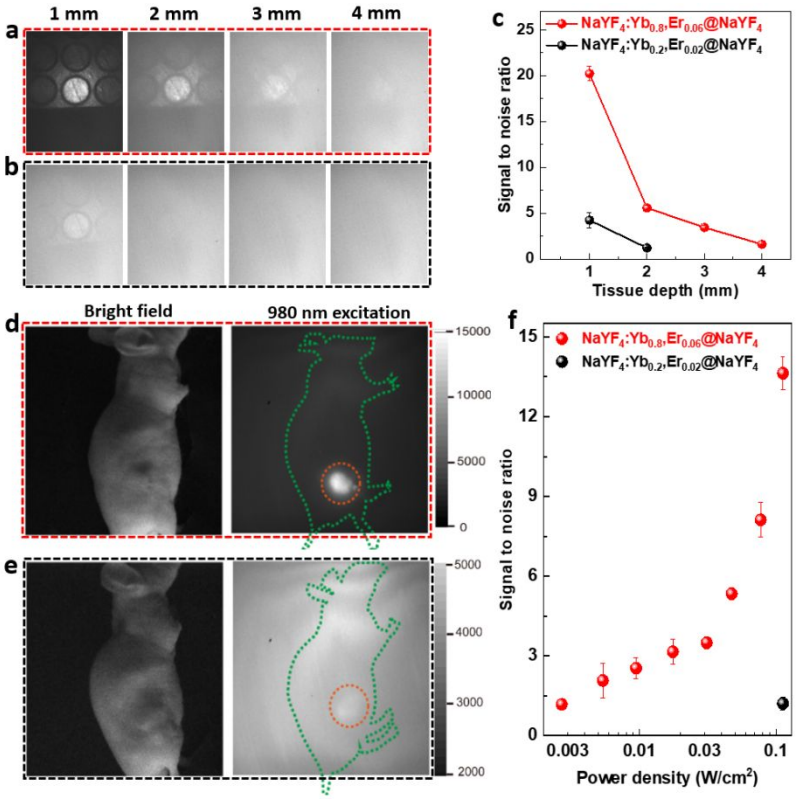

Figure 4. Luminescence imaging of $NaYF_4$:$Yb_{0.8}$,$Er_{0.06}$@$NaYF_4$ (**a**) and $NaYF_4$:$Yb_{0.2}$,$Er_{0.02}$@$NaYF_4$ (**b**) at 660 ± 13 nm under different thickness of pork tissue. (**c**) Quantitative analysis of luminescent signal to noise ratio. In vivo tumor imaging of mice injected with $NaYF_4$:$Yb_{0.8}$,$Er_{0.06}$@$NaYF_4$ (**d**) and $NaYF_4$:$Yb_{0.2}$,$Er_{0.02}$@$NaYF_4$ (**e**) with the 980 nm laser intensity of 0.112 W/cm^2. (**f**) The power-dependent signal to noise ratio of the tumor site injected with the upconversion contrast agents.

To demonstrate $NaYF_4$:$Yb_{0.8}$,$Er_{0.06}$@$NaYF_4$ UCNPs as a more efficient contrast agent for bio imaging, we perform an *in vivo* tumor imaging experiment in the mouse model. As shown in **Fig. 4 d-e**, the tumor site shows an obvious luminescence signals after the administration of $NaYF_4$:$Yb_{0.8}$,$Er_{0.06}$@$NaYF_4$ under the excitation power density of 0.112 W/cm^2, while the tumor site injected with $NaYF_4$:$Yb_{0.2}$,$Er_{0.02}$@$NaYF_4$ only shows a quite weak signal. Further reducing the excitation power, the luminescence signals of both samples becomes weaker (**Fig. S13**). The minimum

excitation laser intensity of 0.112 W/cm^2 is required and the signals are barely distinguished from background for the tumor area injected with $NaYF_4$:$Yb_{0.2}$,$Er_{0.02}$@$NaYF_4$ UCNPs. In contrast, though the irradiance decreases from 0.112 to 0.0027 W/cm^2, the $NaYF_4$:$Yb_{0.8}$,$Er_{0.06}$@$NaYF_4$ UCNPs are still detectable with a SNR of 1.4, as shown in **Fig. 4f**. The new formula of $NaYF_4$:$Yb_{0.8}$,$Er_{0.06}$@$NaYF_4$ UCNPs allows an extremely low excitation power density of 0.0027 W/cm^2 to ignite the marginal area of tumor. This intensity is sufficiently low for their safety usage in the eye region [17], which is potentially useful for mammalian vision repair and enhancement. The reduced dependency of UCNPs on the high excitation power is prospective for non-invasive in vivo imaging to avoid the serious damage in biological tissues.

In conclusion, we identified that 80% Yb^{3+} sensitizers and 6% Er^{3+} activators as the optimal concentrations to yield the highest brightness of UCNPs when mild irradiance of 0.005 to 0.5 W/cm^2 is required for many in vivo bio applications. The optimized formula leads to more than one orders of magnitude enhancements of the upconversion emissions. We further realized the controlled synthesis of 12 nm $NaYF_4$:$Yb_{0.8}$,$Er_{0.06}$@$NaYF_4$ for in vivo tumor imaging with 980 nm excitation irradiance as low as 0.0027 W/cm^2. This work suggests the many recently demonstrated applications of the conventional $NaYF_4$:$Yb_{0.2}$,$Er_{0.02}$@$NaYF_4$ UCNPs in photodynamic therapy, light-triggered drug release, optogenetics, and night vision enhancement will immediately benefit by achieving at least one order of magnitude better performance or significantly reduced power requirement to improve the safety concerns associated with high power irradiance.

Associated Content

Supporting Information

The Supporting Information is available on the ACS Publications website including:

Detailed experiment sections, UCNPs synthesis, TEM images and size distribution histograms, luminescent spectra, integrated luminescent signals, In vitro and in vivo luminescence images

Acknowledgement

We thank S. Lindsay and C. Shen in Microscope Unit at Macquarie University for TEM characterization. This project is financially supported by Australia-China Joint Research Centre for Point-of-Care Testing (ACSRF65827, SQ2017YFGH001190), Science and Technology Innovation Commission of Shenzhen (KQTD20170810110913065), National Natural Science Foundation of

China (NSFC, 61729501, 51720105015). D. L. and Y. L acknowledge the financial support from China Scholarship Council scholarships (Du Li: No. 201506630038; Yongtao Liu: No. 201607950010.)

References

(1) Zhou, B.; Shi, B.; Jin, D.; Liu, X., Controlling upconversion nanocrystals for emerging applications. *Nat. Nanotechnol.* **2015,** *10*, 924.

(2) Dong, H.; Du, S.-R.; Zheng, X.-Y.; Lyu, G.-M.; Sun, L.-D.; Li, L.-D.; Zhang, P.-Z.; Zhang, C.; Yan, C.-H., Lanthanide Nanoparticles: From Design toward Bioimaging and Therapy. *Chem. Rev.* **2015,** *115* (19), 10725-10815.

(3) Yang, D.; Ma, P. a.; Hou, Z.; Cheng, Z.; Li, C.; Lin, J., Current advances in lanthanide ion (Ln3+)-based upconversion nanomaterials for drug delivery. *Chem. Soc. Rev.* **2015,** *44* (6), 1416-1448.

(4) Deng, R.; Qin, F.; Chen, R.; Huang, W.; Hong, M.; Liu, X., Temporal full-colour tuning through non-steady-state upconversion. *Nat. Nanotechnol.* **2015,** *10* (3), 237-242.

(5) Zhou, J.; Wen, S.; Liao, J.; Clarke, C.; Tawfik, S. A.; Ren, W.; Mi, C.; Wang, F.; Jin, D., Activation of the surface dark-layer to enhance upconversion in a thermal field. *Nat. Photon.* **2018,** *12* (3), 154–158.

(6) Zhang, Q.; Yang, F.; Xu, Z.; Chaker, M.; Ma, D., Are lanthanide-doped upconversion materials good candidates for photocatalysis? *Nanoscale Horiz.* **2019**.

(7) Yang, W.; Li, X.; Chi, D.; Zhang, H.; Liu, X., Lanthanide-doped upconversion materials: emerging applications for photovoltaics and photocatalysis. *Nanotechnology* **2014,** *25* (48), 482001.

(8) Zhang, H.; Fan, Y.; Pei, P.; Sun, C.; Lu, L.; Zhang, F., Tm3+-Sensitized NIR-II Fluorescent Nanocrystals for In Vivo Information Storage and Decoding. *Angew. Chem., Int. Ed.* **2019,** *58* (30), 10153-10157.

(9) Liu, Q.; Sun, Y.; Yang, T.; Feng, W.; Li, C.; Li, F., Sub-10 nm Hexagonal Lanthanide-Doped NaLuF4 Upconversion Nanocrystals for Sensitive Bioimaging in Vivo. *J. Am. Chem. Soc.* **2011,** *133* (43), 17122-17125.

(10) Zhou, J.; Liu, Z.; Li, F., Upconversion nanophosphors for small-animal imaging. *Chem. Soc. Rev.* **2012,** *41* (3), 1323-1349.

(11) Fan, Y.; Wang, P.; Lu, Y.; Wang, R.; Zhou, L.; Zheng, X.; Li, X.; Piper, J. A.; Zhang, F., Lifetime-engineered NIR-II nanoparticles unlock multiplexed in vivo imaging. *Nat. Nanotechnol.* **2018,** *13* (10), 941-946.

(12) Wang, S.; Liu, L.; Fan, Y.; El-Toni, A. M.; Alhoshan, M. S.; li, D.; Zhang, F., In Vivo High-resolution Ratiometric Fluorescence Imaging of Inflammation Using NIR-II Nanoprobes with 1550 nm Emission. *Nano Lett.* **2019,** *19* (4), 2418-2427.

(13) Chen, S.; Weitemier, A. Z.; Zeng, X.; He, L.; Wang, X.; Tao, Y.; Huang, A. J. Y.; Hashimotodani, Y.; Kano, M.; Iwasaki, H.; Parajuli, L. K.; Okabe, S.; Teh, D. B. L.; All, A. H.; Tsutsui-Kimura, I.; Tanaka, K. F.; Liu, X.; McHugh, T. J., Near-infrared deep brain stimulation via upconversion nanoparticle–mediated optogenetics. *Science* **2018,** *359* (6376), 679-684.

(14) Idris, N. M.; Gnanasammandhan, M. K.; Zhang, J.; Ho, P. C.; Mahendran, R.; Zhang, Y., In vivo photodynamic therapy using upconversion nanoparticles as remote-controlled nanotransducers. *Nat. Med.* **2012,** *18* (10), 1580-1585.

(15) Nam, S. H.; Bae, Y. M.; Park, Y. I.; Kim, J. H.; Kim, H. M.; Choi, J. S.; Lee, K. T.; Hyeon, T.; Suh, Y. D., Long-Term Real-Time Tracking of Lanthanide Ion Doped Upconverting Nanoparticles in Living Cells. *Angew. Chem., Int. Ed.* **2011,** *50* (27), 6093-6097.
(16) Ximendes, E. C.; Santos, W. Q.; Rocha, U.; Kagola, U. K.; Sanz-Rodríguez, F.; Fernández, N.; Gouveia-Neto, A. d. S.; Bravo, D.; Domingo, A. M.; del Rosal, B.; Brites, C. D. S.; Carlos, L. D.; Jaque, D.; Jacinto, C., Unveiling in Vivo Subcutaneous Thermal Dynamics by Infrared Luminescent Nanothermometers. *Nano Lett.* **2016,** *16* (3), 1695-1703.
(17) Ma, Y.; Bao, J.; Zhang, Y.; Li, Z.; Zhou, X.; Wan, C.; Huang, L.; Zhao, Y.; Han, G.; Xue, T., Mammalian Near-Infrared Image Vision through Injectable and Self-Powered Retinal Nanoantennae. *Cell* **2019,** *177* (2), 243-255.e15.
(18) Wang, F.; Liu, X., Upconversion Multicolor Fine-Tuning: Visible to Near-Infrared Emission from Lanthanide-Doped NaYF4 Nanoparticles. *J. Am. Chem. Soc.* **2008,** *130* (17), 5642-5643.
(19) Krämer, K. W.; Biner, D.; Frei, G.; Güdel, H. U.; Hehlen, M. P.; Lüthi, S. R., Hexagonal Sodium Yttrium Fluoride Based Green and Blue Emitting Upconversion Phosphors. *Chem. Mater.* **2004,** *16* (7), 1244-1251.
(20) Zhao, J.; Jin, D.; Schartner, E. P.; Lu, Y.; Liu, Y.; Zvyagin, A. V.; Zhang, L.; Dawes, J. M.; Xi, P.; Piper, J. A.; Goldys, E. M.; Monro, T. M., Single-nanocrystal sensitivity achieved by enhanced upconversion luminescence. *Nat. Nanotechnol.* **2013,** *8*, 729.
(21) Tian, B.; Fernandez-Bravo, A.; Najafiaghdam, H.; Torquato, N. A.; Altoe, M. V. P.; Teitelboim, A.; Tajon, C. A.; Tian, Y.; Borys, N. J.; Barnard, E. S.; Anwar, M.; Chan, E. M.; Schuck, P. J.; Cohen, B. E., Low irradiance multiphoton imaging with alloyed lanthanide nanocrystals. *Nat. Commun.* **2018,** *9* (1), 3082.
(22) Liu, Q.; Zhang, Y.; Peng, C. S.; Yang, T.; Joubert, L.-M.; Chu, S., Single upconversion nanoparticle imaging at sub-10 W cm−2 irradiance. *Nat. Photon.* **2018,** *12* (9), 548-553.
(23) Ma, C.; Xu, X.; Wang, F.; Zhou, Z.; Liu, D.; Zhao, J.; Guan, M.; Lang, C. I.; Jin, D., Optimal Sensitizer Concentration in Single Upconversion Nanocrystals. *Nano Lett.* **2017,** *17* (5), 2858-2864.
(24) Xia, L.; Kong, X.; Liu, X.; Tu, L.; Zhang, Y.; Chang, Y.; Liu, K.; Shen, D.; Zhao, H.; Zhang, H., An upconversion nanoparticle – Zinc phthalocyanine based nanophotosensitizer for photodynamic therapy. *Biomaterials* **2014,** *35* (13), 4146-4156.
(25) Wang, F.; Wang, J.; Liu, X., Direct Evidence of a Surface Quenching Effect on Size-Dependent Luminescence of Upconversion Nanoparticles. *Angew. Chem., Int. Ed.* **2010,** *49* (41), 7456-7460.
(26) Gargas, D. J.; Chan, E. M.; Ostrowski, A. D.; Aloni, S.; Altoe, M. V. P.; Barnard, E. S.; Sanii, B.; Urban, J. J.; Milliron, D. J.; Cohen, B. E.; Schuck, P. J., Engineering bright sub-10-nm upconverting nanocrystals for single-molecule imaging. *Nat. Nanotechnol.* **2014,** *9*, 300.
(27) Li, X.; Shen, D.; Yang, J.; Yao, C.; Che, R.; Zhang, F.; Zhao, D., Successive Layer-by-Layer Strategy for Multi-Shell Epitaxial Growth: Shell Thickness and Doping Position Dependence in Upconverting Optical Properties. *Chem. Mater.* **2013,** *25* (1), 106-112.
(28) Wen, S.; Zhou, J.; Zheng, K.; Bednarkiewicz, A.; Liu, X.; Jin, D., Advances in highly doped upconversion nanoparticles. *Nat. Commun.* **2018,** *9* (1), 2415.
(29) Punjabi, A.; Wu, X.; Tokatli-Apollon, A.; El-Rifai, M.; Lee, H.; Zhang, Y.; Wang, C.; Liu, Z.; Chan, E. M.; Duan, C.; Han, G., Amplifying the Red-Emission of Upconverting

Nanoparticles for Biocompatible Clinically Used Prodrug-Induced Photodynamic Therapy. *ACS Nano* **2014,** *8* (10), 10621-10630.

(30) Xiong, L.-Q.; Chen, Z.-G.; Yu, M.-X.; Li, F.-Y.; Liu, C.; Huang, C.-H., Synthesis, characterization, and in vivo targeted imaging of amine-functionalized rare-earth up-converting nanophosphors. *Biomaterials* **2009,** *30* (29), 5592-5600.

(31) Garcia, J. V.; Yang, J.; Shen, D.; Yao, C.; Li, X.; Wang, R.; Stucky, G. D.; Zhao, D.; Ford, P. C.; Zhang, F., NIR-Triggered Release of Caged Nitric Oxide using Upconverting Nanostructured Materials. *Small* **2012,** *8* (24), 3800-3805.

(32) Wang, Y.; Lin, X.; Chen, X.; Chen, X.; Xu, Z.; Zhang, W.; Liao, Q.; Duan, X.; Wang, X.; Liu, M.; Wang, F.; He, J.; Shi, P., Tetherless near-infrared control of brain activity in behaving animals using fully implantable upconversion microdevices. *Biomaterials* **2017,** *142*, 136-148.

(33) Li, C.; Xu, L.; Liu, Z.; Li, Z.; Quan, Z.; Al Kheraif, A. A.; Lin, J., Current progress in the controlled synthesis and biomedical applications of ultrasmall (<10 nm) NaREF4 nanoparticles. *Dalton Trans.* **2018,** *47* (26), 8538-8556.

(34) Jin, D.; Xi, P.; Wang, B.; Zhang, L.; Enderlein, J.; van Oijen, A. M., Nanoparticles for super-resolution microscopy and single-molecule tracking. *Nat. Methods* **2018,** *15* (6), 415-423.

TOC

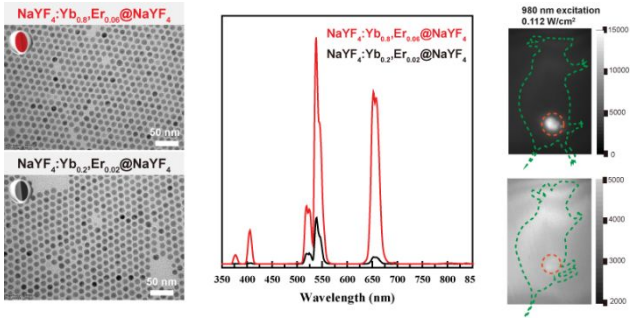
NaYF4:Yb0.8,Er0.06@NaYF4
50 nm
NaYF4:Yb0.2,Er0.02@NaYF4
50 nm
NaYF4:Yb0.8,Er0.06@NaYF4
NaYF4:Yb0.2,Er0.02@NaYF4
350 400 450 500 550 600 650 700 750 800 85
Wavelength (nm)
980 nm excitation
0.112 W/cm2
15000
10000
5000
0
5000
4000
3000
2000